Mapping prefrontal afferents along development

Anne Günther[1*], Malte Stelzer[1*], Andreas Franzelin[2], Annette Marquardt[1], Jan Schröder[2], Thomas Oertner[2], Jastyn A. Pöpplau[1#], Ileana L. Hanganu-Opatz[1#]

[1]Institute of Developmental Neurosciences, Center for Molecular Neurobiology Hamburg, Hamburg Center of Neuroscience, University Medical Center Hamburg-Eppendorf, Falkenried 94, 20251, Hamburg, Germany

[2]Institute of Synaptic Physiology, Center for Molecular Neurobiology Hamburg, Hamburg Center of Neuroscience, University Medical Center Hamburg-Eppendorf, Falkenried 94, 20251, Hamburg, Germany

[*]These authors share first authorship
[#] These authors share last authorship

Corresponding authors: Jastyn A.Pöpplau (Jastyn.poepplau@zmnh.uni-hamburg.de)
Ileana L. Hanganu-Opatz (hangop@zmnh.uni-hamburg.de)

Running title: Development of prefrontal afferents

Keywords: Retrograde labeling, development, neonatal, adolescence, mPFC,corpus callosum, contralateral, myelin, prefrontal afferents

6 Figures
2 Supplementary figures
2 Supplementary tables
24 pages
178 words abstract

SCOPE

Long-range projections allow effective communication between brain regions. In the prefrontal cortex afferent projections comprise inputs that are critical for cognitive, emotional, and social tasks. While structural connectivity patterns of prefrontal afferents in adult animals have been assessed in detail, little is known about their maturation. We provide a detailed examination of region-specific developmental dynamics of prefrontal afferents, assessing ipsi- and contralateral projections. Moreover, we monitor the maturation of axonal myelination at the corpus callosum. These data provide novel insights into the contribution of afferent projections to the protracted development of the prefrontal cortex.

ABSTRACT

The medial prefrontal cortex (mPFC) acts as a hub for cognitive, emotional, and social processes, integrating neuronal inputs from numerous brain regions. Knowledge on the processes underlying formation and myelination of prefrontal afferents is essential for a comprehensive understanding of the emergence, maturation, and refinement of mPFC-dependent behaviors. However, despite detailed investigation of long-range projections to the mPFC in the adult brain, little is known about their maturation. Here, we use retrograde labeling, light-sheet imaging, and automatic cell segmentation to quantify afferent projections to the mPFC from neonatal to adult age. We show that densities of ipsi- and contralateral prefrontal afferents change along development from a widespread bilateral distribution at neonatal age to a precisely tuned, predominantly ipsilateral organization. Furthermore, myelination of interhemispheric prefrontal afferents starts only after the decline of neonatal contralateral projections. We identify specific patterns, *e.g.* elevated projection density from limbic brain regions during early adolescence, or decreasing projection densities from the mediodorsal thalamus decreasing towards adulthood. Overall, these distinct developmental dynamics of prefrontal afferents might have major implications for the maturation of mPFC-dependent functional and behavioral outputs.

GRAPHICAL ABSTRACT

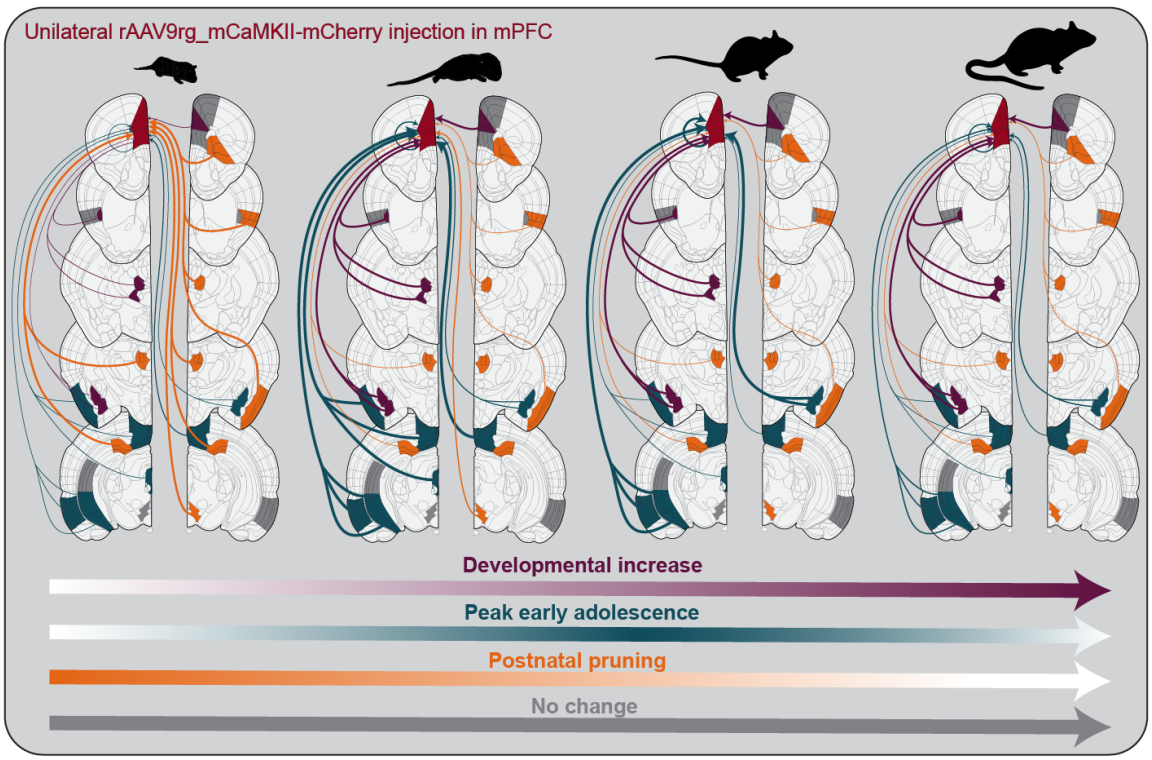

1. INTRODUCTION

The mPFC, a central hub of integrative processing in the brain, is involved in a wide range of cognitive, emotional, and social functions. It integrates direct axonal inputs from numerous cortical and subcortical regions through local and long-range circuits to guide behavior [1–3]. Within the PFC, functions are anatomically and physiologically compartmentalized, with medial subdivisions (*i.e.*, anterior cingulate (ACA), prelimbic (PL), and infralimbic (ILA) areas) primarily contributing to sensorimotor functions, action-planning, and decision making, while ventral regions (*i.e.*, orbitofrontal cortex (ORB)) as well as adjacent cortices (*i.e.*, secondary motor cortices (MOs)) control emotional and motivational behaviors, respectively [4–6]. In contrast, long-range inputs to the mPFC provide essential information on environmental context and internal state from other regions [7,8]. For instance, inputs from the ventromedial thalamus (VM) to the mPFC regulate arousal states [9], while hippocampal projections contribute to working, recognition, and episodic memory [10–13].

However, not only ipsilateral projections shape prefrontal circuits. Interhemispheric connectivity has been shown to increase the complexity of prefrontal networks [14–16]. Numerous studies have investigated the projections crossing the corpus callosum (CC) in rodents and humans [17–19]. While callosal connectivity has been traditionally assumed to be predominantly homotopic (*i.e.*, mPFC to mPFC) [17,20], more recent studies have revealed substantial heterotopy of these projections [21]. Notably, specific functions of homotopic and heterotopic callosal connections have been described in rodents. On the homotopic level, sensory processing has been shown to be influenced by contra- and ipsilateral ACA projections [16], whereas disruptions of heterotopic pathways between basolateral amygdala (BLA) and ACA lead to impaired decision making [14].

In contrast to this detailed dissection of adult prefrontal afferents, little is known about their development. Projections from other brain regions reach the mPFC during development and are thought to undergo dynamic reorganization during early life to promote maturation of higher-order cognitive (*e.g.*, working memory) and emotional functions (*e.g.*, fear learning) [22]. For example, projections from the mediodorsal thalamus (MD) and from the BLA progressively increase in density during development and modulate the maturation of local prefrontal circuits [23–27]. However, prior studies along development have focused on isolated pathways and time points, precluding a large-scale age-dependent mapping of afferents.

In this study, we filled this knowledge gap and systematically monitored the development of axonal projections to the mPFC from birth to adulthood. Using retrograde viral tracing in combination with light-sheet microscopy, we generated a comprehensive atlas of distinct regional afferent projection patterns to the mPFC at different postnatal stages. Based on these results, we used the same retrograde viral tracing approach combined with confocal microscopy to apply automatic cell segmentation for quantification of projecting cells from different regions of the brain. Additionally, we assessed the degree of myelination of retrogradely labeled inputs using immunohistochemical staining of myelin. Our data provide a comprehensive, brain-wide (*i.e.*, ACA, PL, IL, ORB, MOs, agranular insular cortex (AI), piriform cortex (PIRI), BLA, basomedial amygdala (BMA), retrosplenial cortex (RSP), entorhinal cortex (ENT), ventral and intermediate CA1 (CA1v, CA1i), ventral and dorsal subiculum (SUBv, SUBd), claustrum (CLA), anterior nuclei (ATN), VM, MD,

supramammillary nucleus (SUM), periaqueductal gray (PAG), and ventral tegmental area (VTA)) developmental overview, revealing distinct, region- and age-specific dynamics of prefrontal afferent and giving crucial insights into the evolving architecture of prefrontal circuits.

2. MATERIALS AND METHODS

2.1. Animals

All experiments were performed in compliance with German law and guidelines of the European Union for the use of animals in research (European Union Directive 2010/63/EU) and were approved by the local ethical committee (Behörde für Gesundheit und Verbraucherschutz Hamburg). Experiments were carried out in C57BL/6J mice of both sexes. Animals were housed in a 12 h light/12 h dark cycle and were given access to water and food *ad libitum*. The day of birth was considered postnatal day (P) 0.

2.2. Virus Injections

Viral vectors were injected unilaterally into the PFC of the right hemisphere of C57BL/6J mice. Two viral vectors were applied simultaneously: rAAV9rg_mCaMKII-mCherry (#114469-AAVrg, Addgene, Watertown, MA, United States) for retrograde labeling of excitatory projection-neurons and rAAV9_CAG-eGFP (#37825 Addgene, Watertown, MA, United States) for local labeling of cells at the injection site. Viral vectors were prepared in a genome copy ratio of 1:2.5 and injected at the same time using a stereotax [28] (Figure 1A). Viral vectors were injected at four different time points, for which volumes and coordinates were adjusted to compensate for brain volume to result in a comparable virus spread across development, *i.e.* P0 (neonatal, 130 nl at a rate of 120 nl/min, 0.3 mm posterior to the inferior cerebral vein, 0.2 mm lateral to the midline and 0.4-0.8 mm ventral from the brain surface), P10 (pre-juvenile, 170 nl at a rate of 120 nl/min, 1,6 mm anterior to Bregma, 0.2 mm lateral to midline and 0,8-1,2 mm ventral from the brain surface), P20 (juvenile, 190 nl at a rate of 120 nl/min, 1,8 mm anterior to Bregma, 0.2 mm lateral to midline and 1-1,4 mm ventral from the brain surface), and P50 (adult, 210 nl at a rate of 120 nl/min, 1,9 mm anterior to Bregma, 0.2 mm lateral to midline and 1,1-1,5 mm ventral from the brain surface). Mice were transcardially perfused with 4% paraformaldehyde (PFA) 10 days after virus injection, *i.e*. at P10 (neonatal, n=6), P20 (pre-juvenile, n=6), P30 (juvenile, n=6), and P60 (adult, n=6). To further account for differences of viral spread at the injection site, brains were manually categorized as low spread, normal spread, or high spread. Low spread was defined as expression in only one mPFC subdivision or a very low degree of labeled cell bodies in more than one subdivision (neonatal n=1, pre-juvenile n=1). High spread was defined as labeled cell bodies in all three subdivisions of the mPFC, while also slightly exceeding mPFC boundaries on the dorsal-ventral or anterior-posterior axis (neonatal n=1, pre-juvenile n=1, juvenile n=1, adult n=1). Accordingly, normal spread was defined as expression in at least two subdivisions without exceeding mPFC boundaries (neonatal n=4, pre-juvenile n=4, juvenile n=5, adult n=5). Virus spread was included in statistical analysis (see Statistical analysis, Supplementary discussion, and Statistics table S1&2).

2.3. Tissue clearing and light-sheet imaging

Light-sheet imaging on an open source mesoSPIM [29] was used to generate brain-wide overviews of mPFC-projecting brain regions. Perfusion-fixed brains were cleared with SHIELD reagent [30] to preserve endogenous fluorescence and imaged in EasyIndex solution (RI = 1.465, Life Canvas Technologies) with an Orca Flash 4.0 camera (Hamamatsu).

2.4. Cell Quantification

For confocal microscopy, brains were prepared in coronal 100 µm sections and mounted on slides using Vectashield with DAPI (Vector Laboratories, Burlingame, CA, United States). For cell quantification, images were obtained using a confocal microscope (LSN700, Zeiss, Germany) with a 20x objective (2,048 x 2,048 pixels; 319.5 x 319.5 µm). Areas were demarcated according to the coronal P56 mouse reference atlas from the Allen Brain Atlas (mouse.brain-map.org). Additionally, images of mice injected at P0 were also compared to a developing mouse brain atlas (Paxinos et al. 2007). Images of three consecutive coronal brain slices were taken for each brain region in the ipsi- and the contralateral hemispheres. Images were segmented with Cellpose 2 in Python 3.8. using both the standard model algorithm ‘cyto2’ for the images of cells transduced by rAAV9rg_CaMKII-mCherry and a self-trained algorithm as described for the human-in-the-loop approach [31] for rAAV9_CAG-eGFP-transduced cells. After automatic cell segmentation, all images were validated by visual inspection. Confocal images from 22 prefrontal and long-range projecting brain sections with mCherry-labeled pyramidal neurons were quantified as a measure of projection strength to the mPFC across development. Images of eGFP-labeled cells were acquired from prefrontal areas at the injection site (ACA, PL, ILA, ORB, MOs) for normalization of quantification of retrogradely labeled projections. Normalized cell count (NCC) was calculated per brain area using mCherry-labeled cells of a single image from each brain area of an animal (r) and all eGFP-labeled cells of an animal ($\bar{g}$) as: $NCC = \frac{r}{r+\bar{g}}$. Additionally, the mean cell count (x) was calculated as the mean of mCherry-labeled cells from all sections of one region for all animals from all age groups.

2.5. Immunohistochemistry

Immunohistochemical staining of myelin basic protein (MBP) at the CC was performed on the corresponding sections of injected brains after perfusion at P10 (n=4), P20 (n=3), P30 (n=3), and P60 (n=3) as previously described [32]. Briefly, brain slices were permeabilized using 0.8% Triton X-100 (Sigma-Aldrich, MO, USA) and blocked with 5% normal goat serum and 5% normal donkey serum (Jackson Immuno Research, PA, USA) for 1 h. Samples were incubated overnight at 4°C with an MBP antibody (1:500, Abcam ab40390). As a secondary antibody Goat-Anti-Rabbit IgG (H&L) DyLight633-conjugated (1:1000, Agrisera, AS11 1816) was used.

2.6. Myelin Quantification

For myelin quantification, images were obtained using a confocal microscope (Olympus, Tokyo, Japan) with a 60x objective and 2x zoom (1024 x 1024 pixels; 105.47 x 105.47 mm). Immunohistochemically stained samples from injected brains were used to image axonal fibers and myelin at the mid-section of the CC. For every animal, 3-4 stacks from different brain slices (10-30 single images, 150 nm interval) were acquired. After preprocessing and thresholding in ImageJ, colocalization of MBP-positive and mCherry-labeled structures

expression was calculated in Matlab R2023a using a custom-written algorithm similar to [33]. Values were normalized for stack depth.

2.7. Statistical Analysis

Statistical analysis was carried out in R using linear mixed effect models (LME) of the 'lme4' package in R 4.4.1. We assessed the impact of *age* (fixed effect) on NCCs, while accounting for random effects, including *sex*, *viral spread*, and *image number* to consider for multiple image-based measurements per *individual animal*. Analyzed image stacks of myelinated structures, labeled axonal fibers, and their colocalization were similarly analyzed with LME models to determine the effect of fixed and random effects on myelinization of axons. Briefly, likelihood ratio tests were performed to compare log-likelihoods between the full and the reduced model. To test for a significant effect of age-group (fixed effect), sex, or viral spread (random effects), these parameters were removed from the full model to calculate statistical significance using the 'anova' function. Post-hoc pairwise comparisons between age-groups were conducted using the Tukey's Honest Significant Difference test using the 'multcomp' package. P-values were adjusted using the Holm method 'holm' to account for multiple comparisons (see Statistics table S1).

3. RESULTS

3.1. mPFC afferents show age-dependent trajectories

Resolving the developmental dynamics of long-range projections to the mPFC from different brain regions and between hemispheres is the basis for understanding how prefrontal circuits gain and develop their functions. In a first step, we assessed the maturation of prefrontal afferents using light-sheet microscopy on cleared brain tissue. For this, we injected rAAV9rg_mCaMKII-mCherry and rAAV9_CAG-eGFP unilaterally into the mPFC at four different time points (*i.e.*, neonatal P0, pre-juvenile P10, juvenile P20, adult P50). Tissue was perfused and cleared 10 days after injection (*i.e.*, neonatal P10, pre-juvenile P20, juvenile P30, adult P60) (Figure 1A-F). Whole-brain imaging revealed retrogradely labeled cells in multiple cortical and subcortical brain regions of both hemispheres in all mice (Figure 1C, S1). Based on this qualitative overview, we chose 22 brain regions with direct axonal projections to the mPFC along development to analyze in detail. We also included the PAG and VTA (Figure 1C, S1), that showed prominent glutamatergic afferent projections during development but not in the adult brain [1,2]. We used confocal microscopy in slices of injected brains and subsequent cell segmentation (Figure 1D-F) to assess projection strength by calculating the NCC (normalized cell count: calculated as ratio of mCherry-labeled cells from each brain area *vs*. all eGFP- and mCherry-labeled cells, see Materials and Methods section) in prefrontal subdivisions (ACA, PL, ILA, ORB, MOs) as well as in cortical (AI, PIRI, BLA, BMA, RSP, ENT, CA1v, CA1i, SUBv, SUBd) and subcortical areas (CLA, ATN, VM, MD, SUM, PAG, VTA), projecting ipsi- and contralaterally to the mPFC.

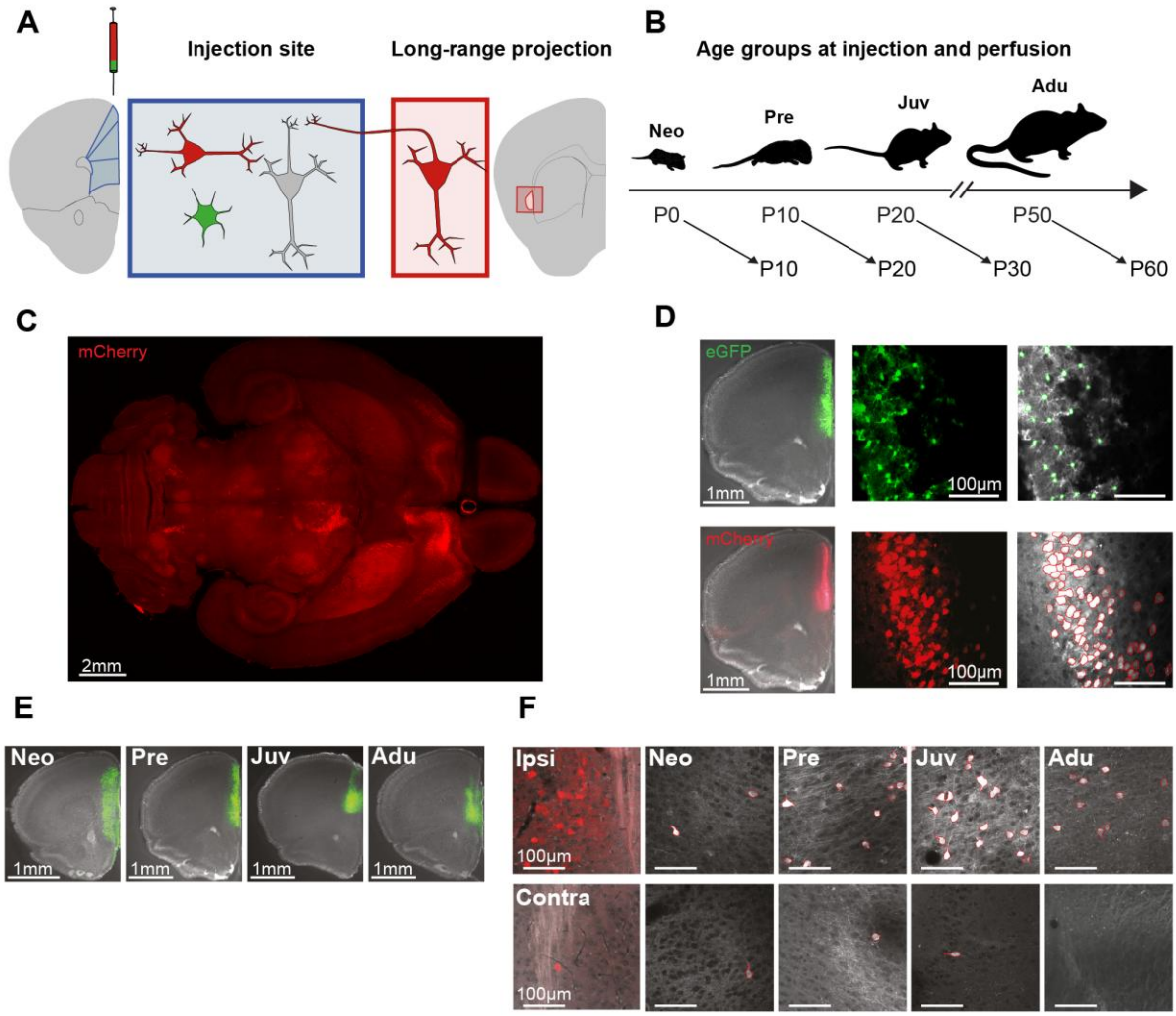

FIGURE 1 | Labeling of mPFC afferents along development. (A) Schematic illustration of the transduction strategy with two viral vectors (rAAV9rg_mCaMKII-mCherry (red) and rAAV9_CAG-eGFP (green)) injected into the right mPFC (left) as well as an example for local and long-range targets (right). **(B)** Schematic of injection and perfusion time points for the four investigated age groups. **(C)** Representative lightsheet microscopy image of a transverse section of a neonatal mouse (P10) with retrograde mCherry labeling (red) shown. **(D)** Representative fluorescence microscope images of a pre-juvenile mouse, depicting the cell detection strategy of both viral constructs at the injection site (left panel: overview, middle panel: fluorescence detected via confocal microscopy, right panel: cell segmentation). **(E)** Representative images of the injection site for all investigated age groups. **(F)** Representative confocal images from the ipsilateral and contralateral CLA of all investigated age groups, depicting the cell detection strategy of retrogradely labeled, long-range projecting cells.

3.2. Medial but not adjacent local prefrontal connectivity increases along development

In order to assess local prefrontal connectivity, we quantified retrogradely labeled cells in prefrontal subdivisions of the ipsilateral hemisphere (marked as ^{i} for all regions). The density of labeled cells in mPFC and adjacent subdivisions changed with age but was not influenced by sex or viral spread (Figure 2A-E). For the ACA^{i} and PL^{i} the NCC increased from neonatal to pre-juvenile age and remained stable afterwards (Figure 2A,B). Solely ILA^{i} local connectivity peaked at juvenile age and decreased in adults (Figure 2C). In contrast, the NCC in adjacent MOs^{i} and ORB^{i} did not significantly change with age (Figure 2D,E). Taken together, these data indicate that especially PL and ILA become strongly integrated into local prefrontal connectivity during development.

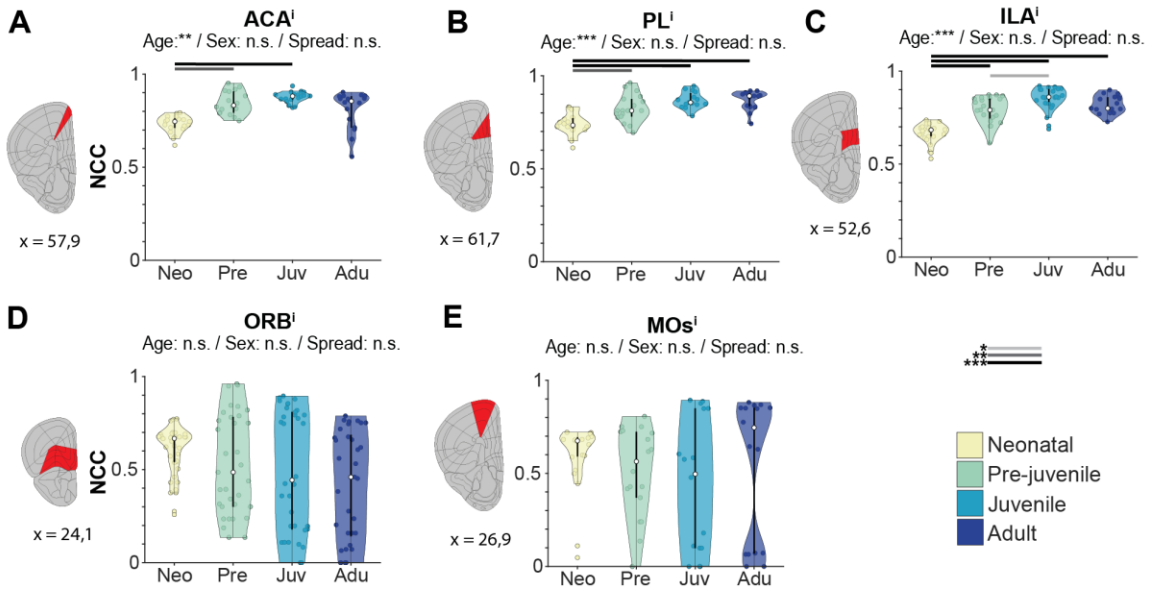

FIGURE 2 | Age-dependent dynamics of local prefrontal connectivity. **(A)** Violin plots displaying the NCC of prefrontally projecting ACA^{i} cells (n = 72 images, 24 mice) for each age group. **(B)** Same as (A) for PL^{i} (n = 67 images, 24 mice). **(C)** Same as (A) for ILA^{i} (n = 83 images, 24 mice). **(D)** Same as (A) for ORB^{i} (n = 136 images, 24 mice). **(E)** Same as (A) for MOs^{i} (n = 70 images, 24 mice). Ipsilateral areas are indicated in red in schematics on the left with mean cell count given as x below sections. Violin plots are represented as median with 25th to 75th percentile. See Statistics table S1 for details.

3.3. Cortical long-range afferents to the mPFC peak at (pre-)juvenile age

Next, we quantified the densities of long-range afferents from ipsilateral cortical (RSP^{i}, PIRI^{i}, AI^{i}, ENT^{i}, SUBv^{i}, SUBd^{i}, CA1i^{i}, and CA1v^{i}) as well as cortical adjacent regions (BLA^{i}, BMA^{i}, CLA^{i}). Sex of investigated mice or viral spread had no confounding effects on the results. In most regions, with exception of AI^{i} that showed a consistently high density of afferents, and CA1i^{i} (Figure 3A,B), prefrontal afferents revealed distinct age-dependent patterns. The densities of projections from BMA^{i}, CLA^{i}, and BLA^{i} strongly increased from neonatal to pre-juvenile age and showed only slight changes later on (Figure 3C-E). Notably, BLA^{i}-to-mPFC afferents were nearly absent at neonatal age, emerging towards pre-juvenile age. A similar pattern, though less striking, was also detected for RSP^{i}, ENT^{i}, and SUBv^{i} (Figure 3F-I,K). However, the densities of these prefrontal afferents decreased during later development, resulting in similar values when comparing neonatal and adult mice. A rather unusual developmental dynamic was detected for SUBd^{i} with dense projections to the mPFC at neonatal age that almost disappeared at adult age (Figure 3J).

Thus, numerous ipsilateral projections target the mPFC during development and reveal distinct dynamics. Overall, long-range connectivity seems to be particularly dense during the pre-juvenile / juvenile period.

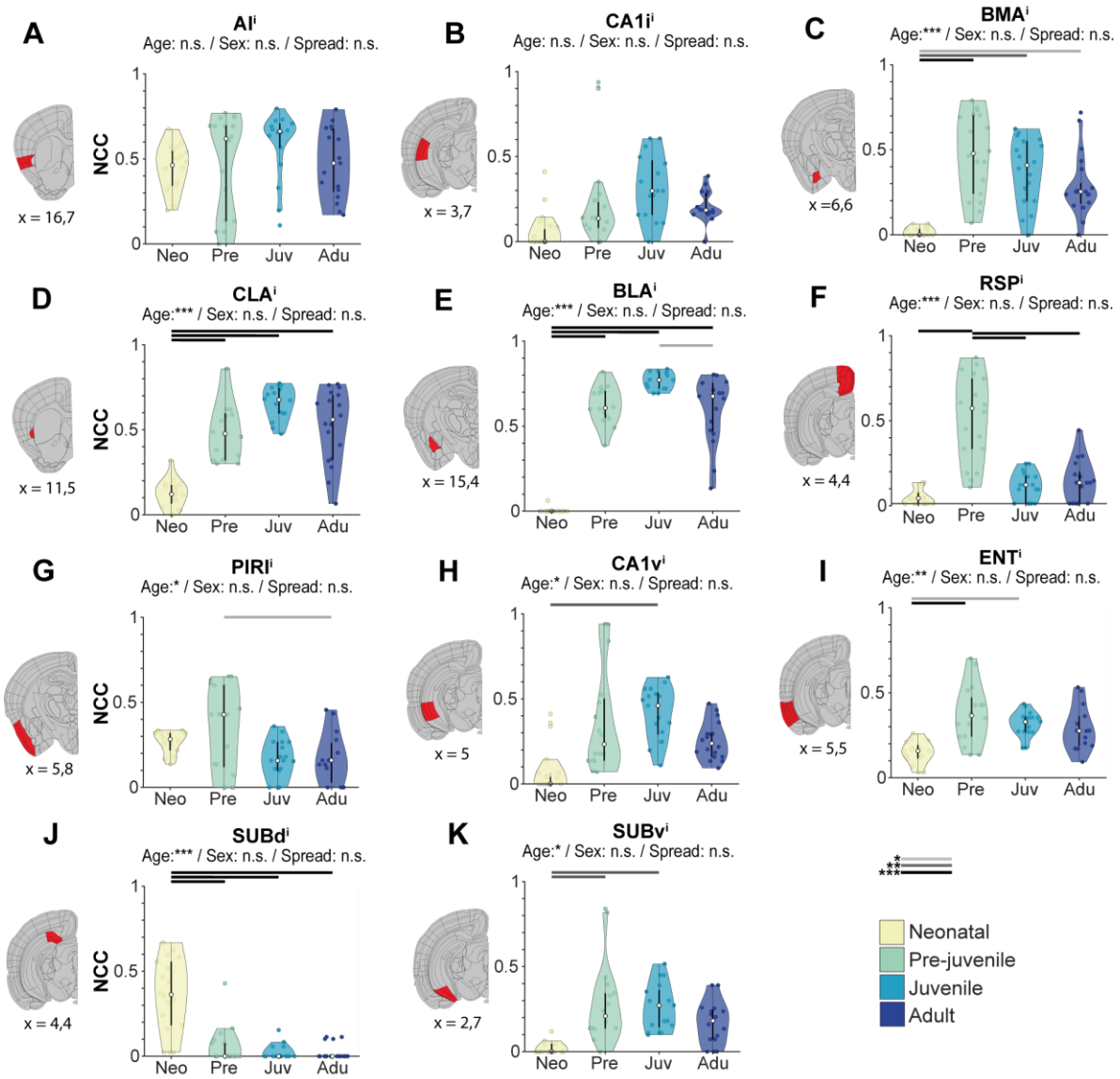

FIGURE 3 | Age-dependent dynamics of cortical and subcortical projections targeting the ipsilateral mPFC. (A) Violin plots displaying the NCC of prefrontally projecting AI^i cells (n = 68 images, 24 mice) for each age group. **(B)** Same as (A) for CA1i^i (n = 67 images, 24 mice). **(C)** Same as (A) for BMA^i (n = 72 images, 24 mice). **(D)** Same as (A) for CLA^i (n = 67 images, 24 mice). **(E)** Same as (A) for BLA^i (n = 70 images, 24 mice). **(E)** Same as (A) for BLA^i (n = 61 images, 24 mice). **(F)** Same as (A) for RSP^i (n = 70 images, 24 mice). **(G)** Same as (A) for PIRI^i (n = 64 images, 24 mice). **(H)** Same as (A) for CA1v^i (n = 69 images, 24 mice). **(I)** Same as (A) for ENT^i (n = 64 images, 24 mice). **(J)** Same as (A) for SUBd^i (n = 70 images, 24 mice). **(K)** Same as (A) for SUBv^i (n = 64 images, 24 mice). Assessed ipsilateral areas are indicated in red in schematics on the left with mean cell count given as x below sections. Violin plots are represented as median with 25th to 75th percentile. See Statistics table S1 for details.

3.4. Prefrontal projections from thalamic and hypothalamic nuclei develop in an inverse manner

Next, we analyzed long-range prefrontal afferents arising from ipsilateral subcortical brain structures (ATN^i, VM^i, MD^i, SUM^i, PAG^i, VTA^i). For the ATN^i, we quantified the interanterodorsal nucleus as well as ventral and dorsal sections of the AM. VTA^i-to-mPFC projections remained unchanged throughout development (Figure 4A). In contrast, the density of VM^i and ATN^i afferents increased from neonatal to pre-juvenile age and remained stable afterwards, even though the density of projections at neonatal age was rather low in VM^i and

high in ATN^{i} (Figure 4B,C). Notably, ATN^{i} was the only region for which we observed an effect of viral spread which decreased with age (see Supplementary discussion, Statistics table S1&S2). The density of labeled cells in the MD^{i} decreased with age, indicating a sparsification of prefrontal afferents (Figure 4D). Similarly, the density of SUM^{i}-to-mPFC projections decreased from pre-juvenile to juvenile age with a significant effect of sex, revealing higher projection densities for male mice (Figure 4E, Statistics table S1&S2). For the PAG^{i}, the density of retrogradely labeled cells was generally low but followed a similar trend as most of the cortical areas and showed a peak at pre-juvenile age (Figure 4F).

Thus, most prefrontal afferents from subcortical regions reach high densities at pre-juvenile age, yet their dynamics, either increasing or decreasing with age, are region-specific.

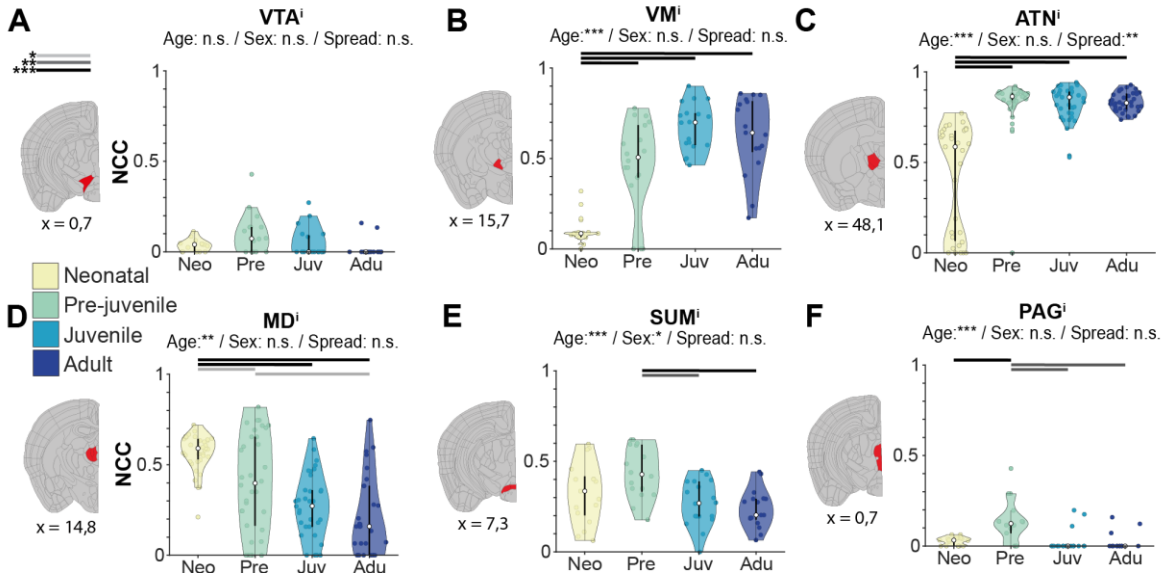

FIGURE 4 | Age-dependent dynamics of projections from midbrain areas targeting the ipsilateral mPFC. **(A)** Violin plots displaying the NCC of prefrontally projecting VTA^{i} cells(n = 63 images, 23 mice) for each age group. **(B)** Same as (A) for VM^{i} (n = 71 images, 24 mice). **(C)** Same as (A) for ATN^{i} (n = 137 images, 24 mice). **(D)** Same as (A) for MD^{i} (n = 135 images, 24 mice). **(E)** Same as (A) for SUM^{i} (n = 68 images, 24 mice). **(E)** Same as (A) for PAG^{i} (n = 62 images, 24 mice). Assessed ipsilateral areas are indicated in red in schematics on the left with mean cell count given as x below sections. Violin plots are represented as median with 25th to 75th percentile. See Statistics table S1&S2 for details.

3.5. Contralateral prefrontal afferents undergo pruning along development

Adult mPFC has been reported to receive afferents from numerous contralateral regions (marked as ^{c} for all regions) (Anastasiades and Carter, 2022). To clarify how these projections evolve along development, we monitored contralateral prefrontal afferents from birth to adulthood alongside ipsilateral projections. While no age-dependent changes of prefrontal afferent density from contralateral ACA^{c}, ILA^{c} and MOs^{c} were detected (Figure S2A), the number of labeled cells in the PL^{c}, similarly to the PL^{i}, increased from neonatal to pre-juvenile age and remained stable afterwards (Figure 5A). In contrast, the number of labeled cells in the ORB^{c} decreased from neonatal to juvenile and adult age (Figure 5B). Whereas projection density from ORB^{i} showed no sex-dependent differences, an effect of sex was detected for the ORB^{c}, the number of labeled cells being higher in male compared to female mice (see Statistics table S2). Other contralateral regions were affected neither by sex nor viral spread.

Based on their observed developmental dynamics, we classified contralateral long-range afferents into four distinct groups. First, afferents that were present at birth and their density remaining constant throughout development. The projections from ENT^c and CLA^c are characteristic for this pattern (Figure 5C; S2A). Second, afferents that were present early during development and strongly decrease later on. This patterns was detected for contralateral afferents from MD^c, RSP^c, AI^c, ATN^c, SUBd^c, PIRI^c, SUM^c, and VTA^c (Figure 5D,E; S2B,C). The RSP^c was the only contralateral brain region for which we detected a density increase of retrogradely-labeled cells from neonatal to pre-juvenile age followed by a substantial decrease at older age (Figure 5E). Similar to the ORB^c, VTA^c was one of the few regions that showed an age-dependent change in contra- but not ipsilateral projections to mPFC (Figure 5B; S2C). Third, the number of retrogradely labeled cells increased with age in a similar manner as their corresponding ipsilateral sections. Afferents from BLA^c and BMA^c belong to this group, despite the density differences between the neonatal and adult group being minor (Figure 5F; S2E). Fourth, almost no prefrontal afferents were detected during the entire development. This pattern was characteristic for CA1v^c, CA1i^c, SUBv^c, VM^c, and PAG^c (Figure S2D).

Taken together, these data reveal that the pruning of contralateral afferents along development follow age- and region-specific patterns, resulting in denser ipsilateral projections from most brain regions to the mPFC at adult age than those from the contralateral hemisphere.

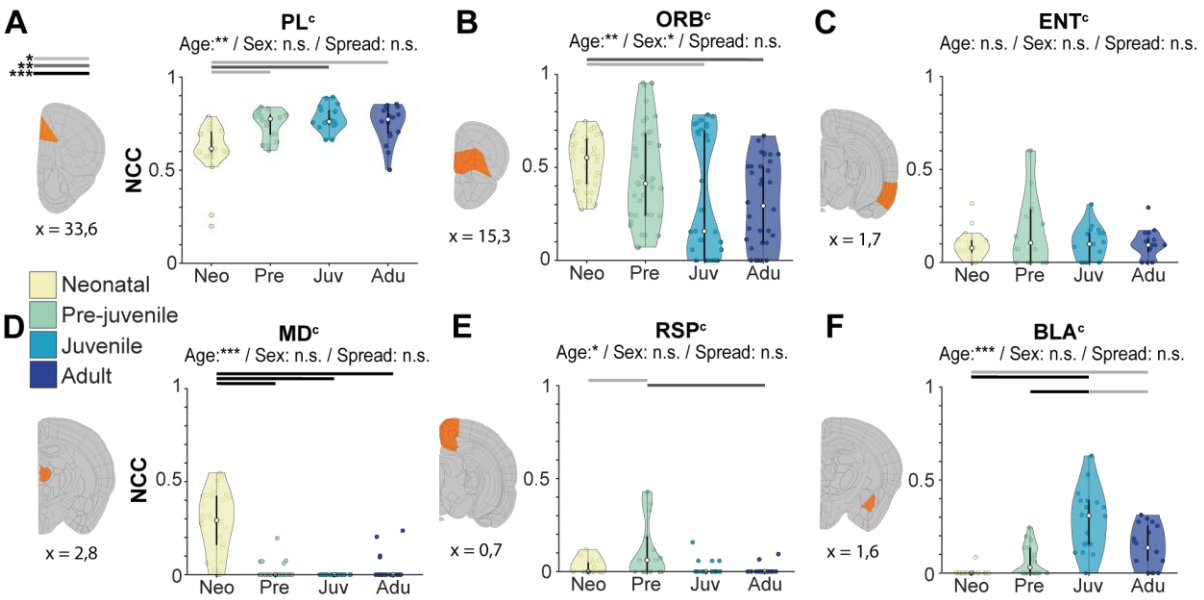

FIGURE 5 | Age-dependent dynamics of contralateral connectivity to the mPFC. **(A)** Violin plots displaying the NCC of prefrontally projecting PL^c cells (n = 72 images, 23 mice) for each age group. **(B)** Same as (A) for ORB^c (n = 139 images, 24 mice). **(C)** Same as (A) for ENT^c (n = 63 images, 23 mice). **(D)** Same as (A) for MD^c (n = 132 images, 24 mice). **(E)** Same as (A) for RSP^c (n = 71 images, 24 mice). **(F)** Same as (A) for BLA^c (n = 70 images, 24 mice). Assessed contralateral areas are indicated in orange in schematics on the left with mean cell count given as x below sections. Violin plots are represented as median with 25th to 75th percentile. See Statistics table S1&S2 for details.

3.6. Myelination of contralateral prefrontal afferents emerges after neonatal age

In addition to monitoring the density of contralateral prefrontal afferents, we also assessed their myelination. For this, we focused on the cortico-cortical projections crossing the CC. The CC represents the largest white matter tract in the mammalian brain [34–36] and it has been extensively

studied at adult age [17–19,35]. We characterized the developmental dynamics of myelination of contralateral prefrontal afferents in the previously defined age groups (neonatal, pre-juvenile, juvenile, and adult) (Figure 6A). Overall myelin expression increased with age (Figure 6B). Retrogradely labeled axons that colocalized with myelin were sparse in neonatal mice, but their density strongly increased at pre-juvenile age and remained elevated until adulthood (Figure 6C). Similarly, the portion of myelin colocalizing with labeled axons increased from neonatal to adult age (Figure 6D).

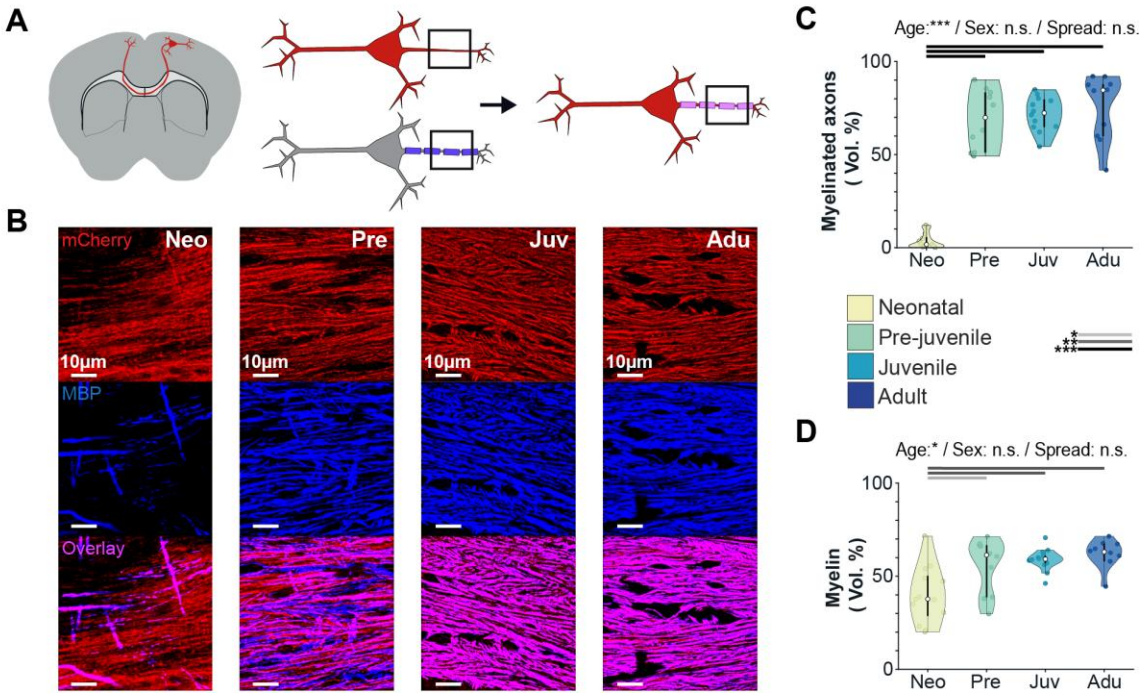

FIGURE 6 | Myelination of hemisphere-crossing prefrontal afferents across age groups. (A) Schematic illustration of myelination quantification strategy of prefrontal afferents crossing the CC. Confocal image stacks (black frames) were acquired from CC, showing mCherry-labeled prefrontal afferents (red) and immunohistochemically stained myelin-sheaths (MBP, blue). Image stacks were overlaid to analyze colocalization (magenta). **(B)** Representative confocal images of labeled axons and myelin sheaths in the CC. Labeled axons (red) and immunohistochemically stained MBP (blue) as well as their overlay (magenta) is shown for each age group. **(C)** Violin plots displaying the volumetric percentage of MBP-overlaid prefrontal afferents normalized to total volume of mCherry-labeled axons for each age group. **(D)** Violin plots displaying the percentage of MBP colocalizing with mCherry-labeled axons normalized to total volume of MBP for each age group (n = 45 images, 13 mice). Violin plots are represented as median with 25th to 75th percentile. See Statistics table S1 for details.

4. DISCUSSION

The PFC is a higher-order cortical region that is essential for complex cognitive and affective processes such as decision making, working memory, and emotional regulation. Its maturation is protracted when compared to primary sensory cortices [22], suggesting a prolonged time window for structural and functional refinement of prefrontal circuits. In this study, we unraveled the developmental dynamics of local and long-range ipsilateral and contralateral projections to the mPFC, with a specific focus on developmental changes in projection strength from different regions (*i.e.*, ACA, PL, IL, ORB, MOs, AI, PIRI, BLA, BMA, RSP, ENT, CA1v, CA1i, SUBv, SUBd, CLA, ATN, VM, MD, SUM, PAG, and VTA) as well as the onset of myelination. Our findings reveal regionally distinct maturational dynamics of prefrontal afferents that might underlie functional and behavioral development.

4.1. Developmental shift from bilateral to unilateral projections to the mPFC

At birth, afferent projections to the mPFC are largely bilateral. However, this pattern shifts progressively towards ipsilateral projections during maturation, with only a subset of cortical and limbic areas retaining contralateral connectivity in adulthood (*i.e.*, ACA^c, PL^c, ILA^c, MOs^c, ORB^c, AI^c, BLA^c, BMA^c, and ENT^c). The most commonly observed dynamic of contralateral projections was a decline of projection density after neonatal age (*i.e.*, ORB^c, AI^c, PIRI^c, SUBd^c, ATN^c, MD^c, SUM^c). While postnatal pruning of perinatal contralateral projections for the ATN and MD has been reported [37,38], our results imply that this unilaterality of prefrontal projections might even be initiated before birth, as contralateral projections at neonatal age are already less dense than ipsilateral ones.

Our data show that myelination of CC-crossing prefrontal afferents begins only after the loss of most contralateral projections. In adult animals, the CC, is the largest white matter tract in the mammalian brain [34,35] and contains mostly cortico-cortical fibers [36], although evidence also suggests the presence of cortico-subcortical connections [20,39]. In line with previous studies [40], we detected low amounts of myelin in the CC and found that mPFC axonal fibers are largely unwrapped at neonatal age. As has been previously shown [41,42], myelination of prefrontal afferents increases strikingly during the second postnatal week, co-occurring with weaning and the onset of more complex behavioral abilities [24]. As oligodendrocyte engagement and axonal wrapping are promoted by activity-dependent mechanisms [43], the absence of myelin in early-stage interhemispheric fibers supports the idea that these projections might lack the necessary activity for functional embedding into mature circuits. In line with this hypothesis, the emergence of activity follows a protracted development in the mPFC [44]. This transient bilateral connectivity may serve as a scaffolding mechanism for the maturation of local prefrontal microcircuits, facilitating early synchronization across hemispheres. The question of whether early contralateral prefrontal projections are functionally active remains to be addressed. Alternatively, these projections could reflect developmental remnants of cerebral ontogenesis that, in the absence of a specific function, are pruned with ongoing maturation.

In line with this, most ipsilaterally projecting regions show an overall increase of input strength from neonatal to adult age, some areas (*e.g.*, MD^i and SUBd^i) demonstrate an overall reduction in mPFC afferents, similar to their contralateral counterparts. This result partially contradicts earlier qualitative, not statistically validated reports, suggesting a rebound of MD input in adulthood [26]. Given the well-established role of the MD in working memory and cognitive functions [27], developmental pruning of its projections to the mPFC appears paradoxical. However, pruning of excessive, non-informative, or redundant projections might improve signal fidelity. Our data suggest that this refinement of projections to the mPFC continues into adulthood, potentially facilitating the emergence of precise, goal-directed behavior.

4.2. Connectivity to the mPFC peaks during early adolescence

One of the most salient observations in our data is the pronounced increase of projections to the mPFC during early adolescence (*i.e.*, pre-juvenile and juvenile group), coinciding with the emergence of higher-order cognitive functions [24,45]. To this point, we could show that afferents

from the limbic regions ENT^{i}, SUBv^{i}, CA1v^{i}, BLA^{i}, BLA^{c}, and BMA^{c} peak in projection strength during early adolescence. For example, the SUBv is known to be involved in the reward circuit of the brain [46] and a role of the CA1 in anticipation of consequences has been proposed [47,48]. Thus, this temporal alignment of projections to the mPFC supports behavioral studies that implicate adolescence as a sensitive window for risk taking and cognitive flexibility in humans [49,50] and in rodents [24,45,51]. Similarly, projections from the amygdala (*i.e.*, BLA and BMA of both hemispheres) are nearly absent in neonatal mice but strongly increase towards pre-juvenile age. This developmental trajectory has been previously described [23] and might be essential for the consolidation of fear memories. Notably, the BLA has also been shown to play a role in decision-making paradigms, in which effort and reward values have to be evaluated [14]. Moreover, increased projection strength from the AM (as part of the ATN^{i}) to the mPFC could facilitate dopamine-dependent reward processing, as its role in reinforcing goal-directed behaviors has been shown in adult mice [52]. Since the density of dopaminergic receptors in the mPFC peaks during adolescence [53], the maturation of these inputs might contribute to the anatomical foundation for adaptive decision-making and behavioral flexibility.

While some brain areas maintained their ipsilateral prefrontal innervations strength after initial increase, other regions showed a decline of projections after early adolescence (*i.e.*, PIRI^{i}, RSP^{i}, and SUM^{i}). These brain regions are associated with olfactory processing, spatial navigation, and episodic memory, all of which become particularly relevant during the transition from maternal dependency to independent exploration [54–56]. The PIRI projects to the ORB as well as to the mPFC [2,57]. These pathways have been reported to be relevant for assessment of food safety [56]. The SUM and RSP are involved in both prefrontal and hippocampal networks and play a role in spatial navigation as well as episodic memory [54,55]. We hypothesize that transient innervation of the early adolescent mPFC by these areas facilitates critical behavioral adaptations at the time of weaning, including food selection and environmental orientation.

4.3. Concluding remarks

In summary, our data reveal that the development of mPFC afferents is neither linear nor uniform but characterized by region-specific dynamics of input formation, stabilization, and pruning (see Supplementary discussion). These anatomical changes closely parallel known milestones of behavioral and functional maturation, suggesting structural development as a framework for functional circuit integration and adult-like cognitive functions. These findings help to understand how early afferent maturation shapes the integrative functions of the mPFC and how disruptions may result in lifelong lasting phenotypes, such as those associated with neurodevelopmental disorders.

5. Conflict of Interest

The authors declare that the research was conducted in the absence of any commercial or financial relationships that could be construed as a potential conflict of interest.

6. Author Contributions

JAP, AG, and ILH-O conceived the study; AG and JAP designed the experiments; MS, AG, JAP, AF, JS, and AM performed the experiments; MS, JAP, and AG analyzed the data; ILH-O, JAP, AG, TO, and MS wrote the paper. All authors have approved the final version of the manuscript.

7. Funding

German Research Foundation FOR5159 Ha4466/20-1 to ILH-O.
German Research Foundation FOR5159 Ha4466/19-1 Start-up fund to JAP and JKK
German Research Foundation Ha4466/23-1 to ILH-O

8. Acknowledgments

We thank P. Putthoff and A. Dahlmann for excellent technical assistance.

9. Data Availability Statement

All data needed to evaluate the conclusions are available in the figures, main text, or the supplementary materials. Raw images are available from the authors upon request.

10. References.

1. Hoover, W.B., and Vertes, R.P. (2007). Anatomical analysis of afferent projections to the medial prefrontal cortex in the rat. Brain Struct. Funct. *212*, 149–179. https://doi.org/10.1007/s00429-007-0150-4.

2. Ährlund-Richter, S., Xuan, Y., van Lunteren, J.A., Kim, H., Ortiz, C., Pollak Dorocic, I., Meletis, K., and Carlén, M. (2019). A whole-brain atlas of monosynaptic input targeting four different cell types in the medial prefrontal cortex of the mouse. Nat. Neurosci. *22*, 657–668. https://doi.org/10.1038/s41593-019-0354-y.

3. Hanganu-Opatz, I.L., Klausberger, T., Sigurdsson, T., Nieder, A., Jacob, S.N., Bartos, M., Sauer, J.-F., Durstewitz, D., Leibold, C., and Diester, I. (2023). Resolving the prefrontal mechanisms of adaptive cognitive behaviors: A cross-species perspective. Neuron *111*, 1020–1036. https://doi.org/10.1016/j.neuron.2023.03.017.

4. Heidbreder, C.A., and Groenewegen, H.J. (2003). The medial prefrontal cortex in the rat: evidence for a dorso-ventral distinction based upon functional and anatomical characteristics. Neurosci. Biobehav. Rev. *27*, 555–579. https://doi.org/10.1016/j.neubiorev.2003.09.003.

5. Laubach, M., Amarante, L.M., Swanson, K., and White, S.R. (2018). What, If Anything, Is Rodent Prefrontal Cortex? eNeuro *5*. https://doi.org/10.1523/ENEURO.0315-18.2018.

6. Anastasiades, P.G., and Carter, A.G. (2021). Circuit organization of the rodent medial prefrontal cortex. Trends Neurosci. *44*, 550–563. https://doi.org/10.1016/j.tins.2021.03.006.

7. Spellman, T., Rigotti, M., Ahmari, S.E., Fusi, S., Gogos, J.A., and Gordon, J.A. (2015). Hippocampal–prefrontal input supports spatial encoding in working memory. Nature *522*, 309–314. https://doi.org/10.1038/nature14445.

8. Burgos-Robles, A., Kimchi, E.Y., Izadmehr, E.M., Porzenheim, M.J., Ramos-Guasp, W.A., Nieh, E.H., Felix-Ortiz, A.C., Namburi, P., Leppla, C.A., Presbrey, K.N., et al. (2017). Amygdala inputs to prefrontal cortex guide behavior amid conflicting cues of reward and punishment. Nat. Neurosci. *20*, 824–835. https://doi.org/10.1038/nn.4553.

9. Honjoh, S., Sasai, S., Schiereck, S.S., Nagai, H., Tononi, G., and Cirelli, C. (2018). Regulation of cortical activity and arousal by the matrix cells of the ventromedial thalamic nucleus. Nat. Commun. *9*, 2100. https://doi.org/10.1038/s41467-018-04497-x.

10. MacDonald, C.J., Lepage, K.Q., Eden, U.T., and Eichenbaum, H. (2011). Hippocampal "Time Cells" Bridge the Gap in Memory for Discontiguous Events. Neuron *71*, 737–749. https://doi.org/10.1016/j.neuron.2011.07.012.

11. Takehara-Nishiuchi, K. (2014). Entorhinal cortex and consolidated memory. Neurosci. Res. *84*, 27–33. https://doi.org/10.1016/j.neures.2014.02.012.

12. Chao, O.Y., Nikolaus, S., Lira Brandão, M., Huston, J.P., and de Souza Silva, M.A. (2017). Interaction between the medial prefrontal cortex and hippocampal CA1 area is essential for episodic-like memory in rats. Neurobiol. Learn. Mem. *141*, 72–77. https://doi.org/10.1016/j.nlm.2017.03.019.

13. Chao, O.Y., de Souza Silva, M.A., Yang, Y.-M., and Huston, J.P. (2020). The medial prefrontal cortex - hippocampus circuit that integrates information of object, place and time to construct episodic memory in rodents: Behavioral, anatomical and neurochemical properties. Neurosci. Biobehav. Rev. *113*, 373–407. https://doi.org/10.1016/j.neubiorev.2020.04.007.

14. Floresco, S.B., and Ghods-Sharifi, S. (2007). Amygdala-Prefrontal Cortical Circuitry Regulates Effort-Based Decision Making. Cereb. Cortex *17*, 251–260. https://doi.org/10.1093/cercor/bhj143.

15. Chao, O.Y., Huston, J.P., Li, J.-S., Wang, A.-L., and de Souza Silva, M.A. (2016). The medial prefrontal cortex-lateral entorhinal cortex circuit is essential for episodic-like memory and associative object-recognition. Hippocampus *26*, 633–645. https://doi.org/10.1002/hipo.22547.

16. Wang, Y., Chen, Z., Ma, G., Wang, L., Liu, Y., Qin, M., Fei, X., Wu, Y., Xu, M., and Zhang, S. (2023). A frontal transcallosal inhibition loop mediates interhemispheric balance in visuospatial processing. Nat. Commun. *14*, 5213. https://doi.org/10.1038/s41467-023-40985-5.

17. Yorke Jr., C.H., and Caviness Jr., V.S. (1975). Interhemispheric neocortical connections of the corpus callosum in the normal mouse: A study based on anterograde and retrograde methods. J. Comp. Neurol. *164*, 233–245. https://doi.org/10.1002/cne.901640206.

18. van der Knaap, L.J., and van der Ham, I.J.M. (2011). How does the corpus callosum mediate interhemispheric transfer? A review. Behav. Brain Res. *223*, 211–221. https://doi.org/10.1016/j.bbr.2011.04.018.

19. Innocenti, G.M., Schmidt, K., Milleret, C., Fabri, M., Knyazeva, M.G., Battaglia-Mayer, A., Aboitiz, F., Ptito, M., Caleo, M., Marzi, C.A., et al. (2022). The functional characterization of callosal connections. Prog. Neurobiol. *208*, 102186. https://doi.org/10.1016/j.pneurobio.2021.102186.

20. De Benedictis, A., Petit, L., Descoteaux, M., Marras, C.E., Barbareschi, M., Corsini, F., Dallabona, M., Chioffi, F., and Sarubbo, S. (2016). New insights in the homotopic and heterotopic connectivity of the frontal portion of the human corpus callosum revealed by microdissection and diffusion tractography. Hum. Brain Mapp. *37*, 4718–4735. https://doi.org/10.1002/hbm.23339.

21. Szczupak, D., Iack, P.M., Rayêe, D., Liu, C., Lent, R., Tovar-Moll, F., and Silva, A.C. (2023). The relevance of heterotopic callosal fibers to interhemispheric connectivity of the mammalian brain. Cereb. Cortex *33*, 4752–4760. https://doi.org/10.1093/cercor/bhac377.

22. Chini, M., and Hanganu-Opatz, I.L. (2021). Prefrontal Cortex Development in Health and Disease: Lessons from Rodents and Humans. Trends Neurosci. *44*, 227–240. https://doi.org/10.1016/j.tins.2020.10.017.

23. Cunningham, M.G., Bhattacharyya, S., and Benes, F.M. (2002). Amygdalo-cortical sprouting continues into early adulthood: implications for the development of normal and abnormal function during adolescence. J. Comp. Neurol. *453*, 116–130. https://doi.org/10.1002/cne.10376.

24. Klune, C.B., Jin, B., and DeNardo, L.A. (2021). Linking mPFC circuit maturation to the developmental regulation of emotional memory and cognitive flexibility. eLife *10*, e64567. https://doi.org/10.7554/eLife.64567.

25. Maren, S., and Quirk, G.J. (2004). Neuronal signalling of fear memory. Nat. Rev. Neurosci. *5*, 844–852. https://doi.org/10.1038/nrn1535.

26. Rios, O., and Villalobos, J. (2004). Postnatal development of the afferent projections from the dorsomedial thalamic nucleus to the frontal cortex in mice. Brain Res. Dev. Brain Res. *150*, 47–50. https://doi.org/10.1016/j.devbrainres.2004.02.005.

27. Parnaudeau, S., Bolkan, S.S., and Kellendonk, C. (2018). The Mediodorsal Thalamus: An Essential Partner of the Prefrontal Cortex for Cognition. Biol. Psychiatry *83*, 648–656. https://doi.org/10.1016/j.biopsych.2017.11.008.

28. Kostka, J.K., and Bitzenhofer, S.H. (2022). Postnatal Development of Centrifugal Inputs to the Olfactory Bulb. Front. Neurosci. *16*. https://doi.org/10.3389/fnins.2022.815282.

29. Voigt, F.F., Kirschenbaum, D., Platonova, E., Pagès, S., Campbell, R.A.A., Kastli, R., Schaettin, M., Egolf, L., van der Bourg, A., Bethge, P., et al. (2019). The mesoSPIM initiative: open-source light-sheet microscopes for imaging cleared tissue. Nat. Methods *16*, 1105–1108. https://doi.org/10.1038/s41592-019-0554-0.

30. Park, Y.-G., Sohn, C.H., Chen, R., McCue, M., Yun, D.H., Drummond, G.T., Ku, T., Evans, N.B., Oak, H.C., Trieu, W., et al. (2019). Protection of tissue physicochemical properties using polyfunctional crosslinkers. Nat. Biotechnol. *37*, 73–83. https://doi.org/10.1038/nbt.4281.

31. Pachitariu, M., and Stringer, C. (2022). Cellpose 2.0: how to train your own model. Nat. Methods *19*, 1634–1641. https://doi.org/10.1038/s41592-022-01663-4.

32. Parbst, F., Kostka, J.K., Günther, A., Chen, Y.-N., Hanganu-Opatz, I.L., and Bitzenhofer, S.H. (2025). Developmental Olfactory Dysfunction and Abnormal Odor Memory in Immune-Challenged Disc1+/− Mice. J. Neurosci. *45*. https://doi.org/10.1523/JNEUROSCI.1007-24.2025.

33. Pöpplau, J.A., Schwarze, T., Dorofeikova, M., Pochinok, I., Günther, A., Marquardt, A., and Hanganu-Opatz, I.L. (2024). Reorganization of adolescent prefrontal cortex circuitry is required for mouse cognitive maturation. Neuron *112*, 421-440.e7. https://doi.org/10.1016/j.neuron.2023.10.024.

34. Fitsiori, A., Nguyen, D., Karentzos, A., Delavelle, J., and Vargas, M.I. (2011). The corpus callosum: white matter or terra incognita. Br. J. Radiol. *84*, 5–18. https://doi.org/10.1259/bjr/21946513.

35. De León Reyes, N.S., Bragg-Gonzalo, L., and Nieto, M. (2020). Development and plasticity of the corpus callosum. Dev. Camb. Engl. *147*, dev189738. https://doi.org/10.1242/dev.189738.

36. Szczupak, D., Iack, P.M., Liu, C., IRC5 Consortium, Tovar-Moll, F., Lent, R., and Silva, A.C. (2021). Direct Interhemispheric Cortical Communication via Thalamic Commissures:

A New White-Matter Pathway in the Rodent Brain. Cereb. Cortex *31*, 4642–4651. https://doi.org/10.1093/cercor/bhab112.

37. Minciacchi, D., and Granato, A. (1989). Development of the thalamocortical system: Transient-crossed projections to the frontal cortex in neonatal rats. J. Comp. Neurol. *281*, 1–12. https://doi.org/10.1002/cne.902810102.

38. De León Reyes, N.S., Mederos, S., Varela, I., Weiss, L.A., Perea, G., Galazo, M.J., and Nieto, M. (2019). Transient callosal projections of L4 neurons are eliminated for the acquisition of local connectivity. Nat. Commun. *10*, 4549. https://doi.org/10.1038/s41467-019-12495-w.

39. Milardi, D., Bramanti, P., Milazzo, C., Finocchio, G., Arrigo, A., Santoro, G., Trimarchi, F., Quartarone, A., Anastasi, G., and Gaeta, M. (2015). Cortical and Subcortical Connections of the Human Claustrum Revealed In Vivo by Constrained Spherical Deconvolution Tractography. Cereb. Cortex *25*, 406–414. https://doi.org/10.1093/cercor/bht231.

40. Sturrock, R.R. (1980). Myelination of the Mouse Corpus Callosum. Neuropathol. Appl. Neurobiol. *6*, 415–420. https://doi.org/10.1111/j.1365-2990.1980.tb00219.x.

41. Paus, T., Zijdenbos, A., Worsley, K., Collins, D.L., Blumenthal, J., Giedd, J.N., Rapoport, J.L., and Evans, A.C. (1999). Structural Maturation of Neural Pathways in Children and Adolescents: In Vivo Study. Science *283*, 1908–1911. https://doi.org/10.1126/science.283.5409.1908.

42. Fornari, E., Knyazeva, M.G., Meuli, R., and Maeder, P. (2007). Myelination shapes functional activity in the developing brain. NeuroImage *38*, 511–518. https://doi.org/10.1016/j.neuroimage.2007.07.010.

43. de Faria, O., Gonsalvez, D.G., Nicholson, M., and Xiao, J. (2019). Activity-dependent central nervous system myelination throughout life. J. Neurochem. *148*, 447–461. https://doi.org/10.1111/jnc.14592.

44. Brockmann, M.D., Pöschel, B., Cichon, N., and Hanganu-Opatz, I.L. (2011). Coupled oscillations mediate directed interactions between prefrontal cortex and hippocampus of the neonatal rat. Neuron *71*, 332–347. https://doi.org/10.1016/j.neuron.2011.05.041.

45. Thies, A.M., Pochinok, I., Marquardt, A., Dorofeikova, M., Hanganu-Opatz, I.L., and Pöpplau, J.A. (2025). Trajectories of working memory and decision making abilities along juvenile development in mice. Front. Neurosci. *19*. https://doi.org/10.3389/fnins.2025.1524931.

46. Ding, S.-L., Yao, Z., Hirokawa, K.E., Nguyen, T.N., Graybuck, L.T., Fong, O., Bohn, P., Ngo, K., Smith, K.A., Koch, C., et al. (2020). Distinct Transcriptomic Cell Types and Neural Circuits of the Subiculum and Prosubiculum along the Dorsal-Ventral Axis. Cell Rep. *31*, 107648. https://doi.org/10.1016/j.celrep.2020.107648.

47. Fyhn, M., Molden, S., Hollup, S., Moser, M.-B., and Moser, E. (2002). Hippocampal neurons responding to first-time dislocation of a target object. Neuron *35*, 555–566. https://doi.org/10.1016/s0896-6273(02)00784-5.

48. Numan, R. (2015). A Prefrontal-Hippocampal Comparator for Goal-Directed Behavior: The Intentional Self and Episodic Memory. Front. Behav. Neurosci. *9*. https://doi.org/10.3389/fnbeh.2015.00323.

49. van Duijvenvoorde, A.C.K., Peters, S., Braams, B.R., and Crone, E.A. (2016). What motivates adolescents? Neural responses to rewards and their influence on adolescents' risk taking, learning, and cognitive control. Neurosci. Biobehav. Rev. *70*, 135–147. https://doi.org/10.1016/j.neubiorev.2016.06.037.

50. McCormick, E.M., and Telzer, E.H. (2018). Not Doomed to Repeat: Enhanced Medial Prefrontal Cortex Tracking of Errors Promotes Adaptive Behavior during Adolescence. J. Cogn. Neurosci. *30*, 281–289. https://doi.org/10.1162/jocn_a_01206.

51. Johnson, C., and Wilbrecht, L. (2011). Juvenile mice show greater flexibility in multiple choice reversal learning than adults. Dev. Cogn. Neurosci. *1*, 540–551. https://doi.org/10.1016/j.dcn.2011.05.008.

52. Yang, C., Hu, Y., Talishinsky, A.D., Potter, C.T., Calva, C.B., Ramsey, L.A., Kesner, A.J., Don, R.F., Junn, S., Tan, A., et al. (2022). Medial prefrontal cortex and anteromedial thalamus interaction regulates goal-directed behavior and dopaminergic neuron activity. Nat. Commun. *13*, 1386. https://doi.org/10.1038/s41467-022-28892-7.

53. Larsen, B., and Luna, B. (2018). Adolescence as a neurobiological critical period for the development of higher-order cognition. Neurosci. Biobehav. Rev. *94*, 179–195. https://doi.org/10.1016/j.neubiorev.2018.09.005.

54. Vann, S.D., Aggleton, J.P., and Maguire, E.A. (2009). What does the retrosplenial cortex do? Nat. Rev. Neurosci. *10*, 792–802. https://doi.org/10.1038/nrn2733.

55. Ito, H.T., Moser, E.I., and Moser, M.-B. (2018). Supramammillary Nucleus Modulates Spike-Time Coordination in the Prefrontal-Thalamo-Hippocampal Circuit during Navigation. Neuron *99*, 576-587.e5. https://doi.org/10.1016/j.neuron.2018.07.021.

56. Loureiro, M., Achargui, R., Flakowski, J., Van Zessen, R., Stefanelli, T., Pascoli, V., and Lüscher, C. (2019). Social transmission of food safety depends on synaptic plasticity in the prefrontal cortex. Science *364*, 991–995. https://doi.org/10.1126/science.aaw5842.

57. Bhattarai, J.P., Etyemez, S., Jaaro-Peled, H., Janke, E., Leon Tolosa, U.D., Kamiya, A., Gottfried, J.A., Sawa, A., and Ma, M. (2022). Olfactory modulation of the medial prefrontal cortex circuitry: Implications for social cognition. Semin. Cell Dev. Biol. *129*, 31–39. https://doi.org/10.1016/j.semcdb.2021.03.022.